Thermodynamics of low-dimensional spin-$\frac{1}{2}$ Heisenberg ferromagnets in an external magnetic field within a Green function formalism

T. N. Antsygina, M. I. Poltavskaya, I. I. Poltavsky, and K. A. Chishko*
B. Verkin Institute for Low Temperature Physics and Engineering, 47 Lenin Avenue, 61103 Kharkov, Ukraine
(Received 27 June 2007; published 9 January 2008)

The thermodynamics of low-dimensional spin-$\frac{1}{2}$ Heisenberg ferromagnets (HFMs) in an external magnetic field is investigated within a second-order two-time Green function formalism in the wide temperature and field ranges. A crucial point of the proposed scheme is a proper account of the analytical properties for the approximate transverse commutator Green function obtained as a result of the decoupling procedure. A good quantitative description of the correlation functions, magnetization, susceptibility, and heat capacity of the HFMs on a chain and square and triangular lattices is found for both infinite- and finite-sized systems. The dependences of the thermodynamic functions of two-dimensional HFMs on the cluster size are studied. The obtained results agree well with the corresponding data found by Bethe ansatz, exact diagonalization, high temperature series expansions, and quantum Monte Carlo simulations.

DOI: 10.1103/PhysRevB.77.024407 PACS number(s): 75.40.Cx

I. INTRODUCTION

The quantum Heisenberg model with ferromagnetic exchange is used extensively to interpret the thermodynamic and magnetic properties of low-dimensional [one-dimensional (1D) and two-dimensional (2D)] physical systems. Examples of quasi-one-dimensional ferromagnets whose properties can be explained within the Heisenberg model are organic p-NPNN compounds[1–5] and cuprates TMCuC.[6,7] The ferromagnetic insulators, such as K_2CuF_4, Cs_2CuF_4, La_2BaCuO_5, and Rb_2CrCl_4,[8–10] and quantum Hall ferromagnets[11–13] provide examples of the Heisenberg system on a square lattice. A unique example of a spin-$\frac{1}{2}$ magnet on a triangular lattice is ^{3}He bilayers adsorbed on graphite.[14–21] At high coverages, the second layer proved to be a solid ferromagnet whose thermodynamics can be described by a Heisenberg ferromagnet (HFM) with a high degree of accuracy.[21–25] Nowadays, considerable study is being given to ^{3}He monolayers on ^{4}He-preplated graphite substrates. In these systems under high enough pressure, a solid ^{3}He monolayer with ferromagnetic exchange is formed.[26,27]

Experimental research of the aforementioned low-dimensional magnets is carried out intensively, in particular, in the presence of an external magnetic field. To interpret the experimental data, it is necessary to develop a quantitative description of the HFM thermodynamics at arbitrary magnetic fields and temperatures. The two-time Green function formalism is quite appropriate for this purpose. The method based on one or another decoupling scheme for higher Green functions results in a closed set of self-consistent equations for thermodynamic averages.[28–31] Random phase approximation (RPA) is the simplest variant of such a scheme with decoupling at the first step.[32] Being applied to the low-dimensional systems, it gives satisfactory results at high fields, whereas at low and intermediate fields, RPA describes the thermodynamics only on a qualitative level.

A quantitative description of 1D and 2D spin systems can be obtained within a more complicated scheme originally proposed in Ref. 33 for a 1D HFM in zero magnetic field. The scheme is based on the decoupling of higher Green functions at the second step with the introduction of the vertex parameters to be found. A proper choice of the vertex parameters makes it possible to retain some relations that must hold true at the exact solving of the problem. As a result, the theory is built in terms of the correlation functions and the vertex parameters obeying the self-consistent set of equations. In Refs. 33–38, a single vertex parameter was chosen so as to satisfy the sum rule. One vertex parameter turned out to be quite enough to describe quantitatively the thermodynamics of 1D and 2D (on square and triangular lattices) ferromagnets in zero field.

When employing the above-mentioned scheme to the spin systems in an external magnetic field, along with the correlators, we have to determine at least three additional functions of temperature and field: two vertex parameters and magnetization. To do this, we need three relations, two of which are quite evident from the properties of the spin-$\frac{1}{2}$ operator

$$\langle (S^z)^2 \rangle = \frac{1}{4}, \quad \langle S^z \rangle = \frac{1}{2} - \langle S^- S^+ \rangle, \tag{1}$$

where angular brackets denote thermodynamic averaging. The choice of the third condition is not so apparent. In Ref. 39, a second-order Green function scheme was applied to a HFM chain and a HFM on a square lattice. As the third condition, Junger *et al.*[39] used the exact representation of the internal energy through the transverse Green function.[30,32]

The aim of the present work is to calculate the thermodynamic functions of a HFM on a triangular lattice in an external magnetic field using a second-order Green function formalism. As compared to a chain and a square lattice,[12,39–42] a HFM on a triangular lattice in a magnetic field is much less investigated. For this case, high-temperature series expansion (HTSE),[43] low-temperature asymptotics for the magnetization calculated within the spin wave approximation,[44,45] temperature dependences of the magnetization found by quantum Monte Carlo simulations (QMCs) on a 16×16 cluster,[44] and some results obtained by the renormalization group technique[46] (RGT) are known. However, none of these approaches gives a complete description of the thermody-

namics in the whole temperature and field ranges, and a second-order Green function method is expected to fill the gap.

In the present work, we show that this method is more effective when the conditions determining the magnetization and vertex parameters result from the fundamental principles. Clearly, the relations (1) are just of this kind. It is equally important to retain the analytical properties[28,30,31] of the Green functions in the approximate approach. Such a requirement for the transverse commutator Green function provides a basis for the third condition in our theory. Note also that by an appropriate choice of variables, the set of self-consistent equations for the correlators, vertex parameters, and magnetization can be written in a universal form suited not only for a triangular lattice but also for a chain and a square lattice. Good agreement of our results obtained for the three types of lattices with the corresponding data available from literature confirms the efficiency of the scheme used.

In Sec. II, the statement of the problem is formulated, and the self-consistent set of equations for the correlators, magnetization, and vertex parameters is derived. In Sec. III, the proposed scheme is applied to a HFM on a chain and square and triangular lattices. The obtained results are compared with the corresponding data found within other methods. Some concluding remarks are made in Sec. IV.

II. STATEMENT OF THE PROBLEM

The Hamiltonian of the system is given by

$$H = -\frac{J}{2}\sum_{\mathbf{f},\boldsymbol{\delta}} \mathbf{S}_{\mathbf{f}}\mathbf{S}_{\mathbf{f}+\boldsymbol{\delta}} - h\sum_{\mathbf{f}} S^z_{\mathbf{f}}, \tag{2}$$

where $\mathbf{S}_{\mathbf{f}}$ is the spin-half operator at site $\mathbf{f}$, $\boldsymbol{\delta}$ is a vector connecting nearest neighbors, $J>0$ is an exchange integral, and $h=2\mu B$, where μ is the magnetic moment of a particle and B is an external magnetic field.

To calculate spin-spin correlators, it is necessary to find two retarded commutator single-particle Green functions: $\langle\langle S^z_{\mathbf{f}} | S^z_{\mathbf{f}'}\rangle\rangle$, $\langle\langle S^{\sigma}_{\mathbf{f}} | S^{-\sigma}_{\mathbf{f}'}\rangle\rangle$ ($\sigma=\pm$). We write down equations of motion for these two functions and make the decoupling of the higher Green functions on the second step according to the scheme proposed in Ref. 39,

$$S^{\sigma}_i S^{\sigma}_j S^{-\sigma}_l = \alpha_{\perp}(\langle S^{\sigma}_j S^{-\sigma}_l\rangle S^{\sigma}_i + \langle S^{\sigma}_i S^{-\sigma}_l\rangle S^{\sigma}_j),$$

$$S^z_i S^z_j S^{\sigma}_l = \alpha_{\perp}\langle S^z_i S^z_j\rangle S^{\sigma}_l, \quad S^{\sigma}_i S^{-\sigma}_j S^z_l = \alpha_z \langle S^{\sigma}_i S^{-\sigma}_j\rangle S^z_l,$$

$$i \neq j \neq l, \quad i \neq l, \tag{3}$$

where $\alpha_{\perp}$ and α_z are the vertex parameters.

After a number of manipulations, we finally obtain for the time-space Fourier component

$$\langle\langle S^z_{\mathbf{k}} | S^z_{-\mathbf{k}}\rangle\rangle_{\omega} = \frac{Jc_1\gamma_0}{4\pi}\frac{1-\Gamma_{\mathbf{k}}}{\omega^2 - (\omega^z_{\mathbf{k}})^2}, \tag{4}$$

where

$$(\omega^z_{\mathbf{k}})^2 = \frac{J^2\gamma_0}{2}(1-\Gamma_{\mathbf{k}})[\Delta_z + \gamma_0\tilde{c}_1(1-\Gamma_{\mathbf{k}})], \tag{5}$$

$$\Delta_z = 1 + \tilde{c}_2 - (\gamma_0+1)\tilde{c}_1. \tag{6}$$

Here, the following correlation functions have been introduced:

$$c_1 = 2\langle S^{\sigma}_{\mathbf{f}} S^{-\sigma}_{\mathbf{f}+\boldsymbol{\delta}}\rangle, \quad c_2 = 2\sum_{\boldsymbol{\delta}}{}' \langle S^{\sigma}_{\mathbf{f}+\boldsymbol{\delta}} S^{-\sigma}_{\mathbf{f}+\boldsymbol{\delta}'}\rangle, \quad \tilde{c}_{1,2} = \alpha_z c_{1,2}. \tag{7}$$

The primed sum indicates that the term with $\boldsymbol{\delta}=\boldsymbol{\delta}'$ is omitted in it. The structure factor $\Gamma_{\mathbf{k}}$ is defined as

$$\Gamma_{\mathbf{k}} = \frac{1}{\gamma_0}\sum_{\boldsymbol{\delta}} \exp(i\mathbf{k}\boldsymbol{\delta}), \tag{8}$$

where the coordination number γ_0 is equal to 2 for a chain, 4 for a square lattice, and 6 for a triangular lattice.

Fourier transform $\langle\langle S^{\sigma}_{\mathbf{k}} | S^{-\sigma}_{-\mathbf{k}}\rangle\rangle_{\omega}$ can be written as

$$\langle\langle S^{\sigma}_{\mathbf{k}} | S^{-\sigma}_{-\mathbf{k}}\rangle\rangle_{\omega} = \frac{1}{2\pi}\sum_{l=1,2}\frac{A^{\sigma}_{l,\mathbf{k}}}{\omega - \Omega^{\sigma}_{l,\mathbf{k}}}. \tag{9}$$

Here,

$$\Omega^{\sigma}_{l,\mathbf{k}} = h\sigma + (-1)^l\omega^{\perp}_{\mathbf{k}}, \tag{10}$$

$$(\omega^{\perp}_{\mathbf{k}})^2 = \frac{J^2\gamma_0}{2}(1-\Gamma_{\mathbf{k}})[\Delta_{\perp} + \gamma_0\tilde{b}_1(1-\Gamma_{\mathbf{k}})], \tag{11}$$

$$\Delta_{\perp} = 1 + \tilde{b}_2 - (\gamma_0+1)\tilde{b}_1, \tag{12}$$

$$A^{\sigma}_{l,\mathbf{k}} = \sigma\langle S^z\rangle + \frac{(-1)^l Jb_1\gamma_0}{2\omega^{\perp}_{\mathbf{k}}}(1-\Gamma_{\mathbf{k}}), \tag{13}$$

where $\langle S^z\rangle$ is the magnetization. Due to the presence of the external magnetic field, $\langle S^z\rangle$ is nonzero at any finite temperature.

The correlation functions entering Eqs. (11)–(13) are defined by

$$b_l = \frac{a_l + c_l}{2}, \quad \tilde{b}_l = \alpha_{\perp} b_l, \quad l = 1 \quad \text{or } 2, \tag{14}$$

$$a_1 = 4\langle S^z_{\mathbf{f}} S^z_{\mathbf{f}+\boldsymbol{\delta}}\rangle, \quad a_2 = 4\sum_{\boldsymbol{\delta}}{}' \langle S^z_{\mathbf{f}+\boldsymbol{\delta}} S^z_{\mathbf{f}+\boldsymbol{\delta}'}\rangle. \tag{15}$$

The Green functions look formally the same for the three above-mentioned types of lattices. Such a universal form has been possible to obtain, because instead of the usual correlators describing correlations between spins which are two steps along the translation vector $\boldsymbol{\delta}$ apart, we use linear combinations c_2 and a_2 defined by Eqs. (7) and (15). The physical meaning of these combinations depends on the lattice type. For a chain, c_2 and a_2 are the next nearest neighbor correlators. For a square lattice, these combinations contain the correlation functions between the spin at site $\mathbf{f}$ and spins from the second and third coordination spheres. For a triangular lattice, these combinations, in addition to the higher order correlators, include also c_1 and a_1. For a chain and a square lattice, Green functions (4) and (9) coincide with those found in Ref. 39.

Using the spectral relations,[28] we have

$$a_1 = \frac{Jc_1}{N}\sum_{\mathbf{k}} \Gamma_{\mathbf{k}} g_{\mathbf{k}} + 4\langle S^z\rangle^2,$$

$$a_2 = \frac{Jc_1}{N}\sum_{\mathbf{k}} (\gamma_0\Gamma_{\mathbf{k}}^2 - 1) g_{\mathbf{k}} + 4(\gamma_0 - 1)\langle S^z\rangle^2,$$

$$c_1 = \frac{1}{\alpha_\perp N}\sum_{\mathbf{k}} \Gamma_{\mathbf{k}} p_{\mathbf{k}},$$

$$c_2 = \frac{1}{\alpha_\perp N}\sum_{\mathbf{k}} (\gamma_0\Gamma_{\mathbf{k}}^2 - 1) p_{\mathbf{k}}, \tag{16}$$

where

$$g_{\mathbf{k}} = \frac{\gamma_0}{\omega_{\mathbf{k}}^z}(1 - \Gamma_{\mathbf{k}})\coth\left(\frac{\beta\omega_{\mathbf{k}}^z}{2}\right),$$

$$p_{\mathbf{k}} = \frac{2\alpha_\perp\langle S^z\rangle\sinh(\beta h) - J\tilde{b}_1\gamma_0(1 - \Gamma_{\mathbf{k}})\sinh(\beta\omega_{\mathbf{k}}^\perp)/\omega_{\mathbf{k}}^\perp}{\cosh(\beta h) - \cosh(\beta\omega_{\mathbf{k}}^\perp)}, \tag{17}$$

N is the total number of sites, and $\beta = 1/T$. Equation (16) represents the set of equations for the correlation functions c_l and a_l. Along with these correlators, the set (16) contains the parameters α_z and $\alpha_\perp$, and magnetization $\langle S^z\rangle$ to be also determined.

The vertex parameters are chosen so as to satisfy the sum rules

$$4\langle (S_{\mathbf{f}}^z)^2\rangle = 1, \quad 2\langle S_{\mathbf{f}}^\sigma S_{\mathbf{f}}^{-\sigma}\rangle = 1 + 2\sigma\langle S^z\rangle,$$

which, using Eq. (17), can be written as

$$\frac{Jc_1}{N}\sum_{\mathbf{k}} g_{\mathbf{k}} + 4\langle S^z\rangle^2 = 1, \quad \alpha_\perp = \frac{1}{N}\sum_{\mathbf{k}} p_{\mathbf{k}}. \tag{18}$$

Finally, in order to close the system (16) and (18), we need one more equation. It can be found from the following consideration. It is known[28,30] that a commutator Green function must not have any pole at $\omega = 0$. Clearly, Green function (4) does not have such a pole. A different situation arises with Green function (9). When $\omega = 0$, its denominator is equal to zero at $\mathbf{k} = \mathbf{k}_0$, with wave vector $\mathbf{k}_0$ satisfying the equation

$$h = \omega_{\mathbf{k}_0}^\perp. \tag{19}$$

Thus, the numerator of Green function (9) must also vanish at $\mathbf{k} = \mathbf{k}_0$; otherwise, this function would have a pole. From this condition, we get the equation for $\langle S^z\rangle$:

$$\langle S^z\rangle = \frac{Jb_1\gamma_0}{2\omega_{\mathbf{k}_0}^\perp}(1 - \Gamma_{\mathbf{k}_0}). \tag{20}$$

Note that in calculating the anticommutator transverse Green function, the condition (20) appears automatically without any special assumptions (see also Ref. 31).

Let us analyze Eq. (19). The frequency $\omega_{\mathbf{k}}^\perp$ has a maximum $\omega_{max}^\perp$ at the edge of the Brillouin zone,

$$(\omega_{max}^\perp)^2 = \gamma_0 J^2(\Delta_\perp + 2\gamma_0\tilde{b}_1). \tag{21}$$

Since the parameters $\Delta_\perp$ and $\tilde{b}_1$ in Eq. (21) are functions of temperature, the frequency $\omega_{max}^\perp$ depends on temperature as well. It can be shown that $\omega_{max}^\perp$ decreases monotonically from $\omega_{max}^\perp = J\gamma_0$ at $T = 0$ to $\omega_{max}^\perp = J\sqrt{\gamma_0}$ at $T \to \infty$. At $h/J < \sqrt{\gamma_0}$, Eq. (19) has a real solution for any temperature. Substituting it into Eq. (20), we obtain the following expression for the magnetization:

$$\langle S^z\rangle = \frac{J}{4h\alpha_\perp}\left(\sqrt{\Delta_\perp^2 + \frac{8h^2\tilde{b}_1}{J^2}} - \Delta_\perp\right). \tag{22}$$

In the field range $\sqrt{\gamma_0} < h/J < \gamma_0$, the real solution of Eq. (19) exists only at $T < T_0$ [where T_0 obeys the equation $\omega_{max}^\perp(T_0) = h$]. Finally, if $h/J > \gamma_0$, Eq. (19) has no real solutions at any temperature.

It is natural to suppose that the expression (22) for the magnetization is valid at arbitrary h and T. This assumption provides continuity of $\langle S^z\rangle$ as a function of field and temperature. Equation (22) gives correct values of the magnetization at low and high fields for arbitrary temperatures and at $T = 0$ for arbitrary fields. However, the most important thing is that Eq. (22) provides correct analytical properties of the commutator Green function (9) obtained within the approximate scheme.

As a result, Eqs. (16), (18), and (22) represent a closed set of seven self-consistent equations for a_1, a_2, c_1, c_2, α_z, $\alpha_\perp$, and $\langle S^z\rangle$. This set can be reduced to three equations for $\tilde{b}_1$, Δ_z, and $\Delta_\perp$

$$1 = \frac{Jc_1}{N}\sum_{\mathbf{k}} g_{\mathbf{k}} + 4\langle S^z\rangle^2,$$

$$2\tilde{b}_1 = \alpha_\perp c_1\left[1 - \frac{J}{N}\sum_{\mathbf{k}} (1 - \Gamma_{\mathbf{k}}) g_{\mathbf{k}}\right] + \alpha_\perp,$$

$$\Delta_\perp = 1 - \alpha_\perp + \frac{\alpha_\perp}{2\alpha_z}(\Delta_z - 1) + \frac{J\alpha_\perp c_1}{2N}\sum_{\mathbf{k}} (1 - \Gamma_{\mathbf{k}})(1 - \gamma_0\Gamma_{\mathbf{k}}) g_{\mathbf{k}}. \tag{23}$$

The values c_1, $\alpha_\perp$, and $\langle S^z\rangle$ can be expressed through $\tilde{b}_1$, Δ_z and $\Delta_\perp$ according to Eqs. (16), (18), and (22). For α_z, with the help of Eqs. (6) and (7), we have

$$\alpha_z = \frac{1 - \Delta_z}{(\gamma_0 + 1)c_1 - c_2}. \tag{24}$$

It is easy to see that the replacement $h \to -h$ changes the sign of the magnetization and does not change the correlation functions and vertex parameters. Owing to condition (22), Eq. (17) and thereby Eqs. (16) and (18) have no singularities. At $h = 0$, the system (23) reduces to that found in Refs. 33 and 38.

The internal energy E per site is given by

$$E = -\frac{J\gamma_0}{8}(2c_1 + a_1) - h\langle S^z\rangle. \tag{25}$$

The efficiency of the proposed scheme can be estimated, first, by comparing the obtained results with those available from literature data found by alternative methods, and, second, with the help of inherent criteria existing within the developed scheme itself. The first criterion implies that at $T\to\infty$, the entropy (per site) of the system with spin-$\frac{1}{2}$ should tend to $S(\infty)=\ln 2\approx 0.693$.

The second criterion follows from the relation[30] connecting the internal energy (25) and the Green function $\langle\langle S_{\mathbf{k}}^{+}|S_{-\mathbf{k}}^{-}\rangle\rangle_{\omega}$, which can be written as

$$\frac{J\gamma_0}{8}(2c_1+a_1-1)+h\left(\langle S^z\rangle-\frac{1}{2}\right)$$
$$-\frac{1}{N}\sum_{\mathbf{k}}\int_{-\infty}^{\infty}d\omega\frac{(\varepsilon_{\mathbf{k}}+\omega)\mathrm{Im}\langle\langle S_{\mathbf{k}}^{+}|S_{-\mathbf{k}}^{-}\rangle\rangle_{\omega}}{e^{\beta\omega}-1}=0, \quad (26)$$

where $\varepsilon_{\mathbf{k}}=J\gamma_0(1-\Gamma_{\mathbf{k}})/2+h$. The relation (26) becomes the identity with the exact Green function and correlators. This is not the case for the Green function and correlators found as a result of the decoupling procedure. Dividing Eq. (26) by $J\gamma_0\langle S^z\rangle/4$ and substituting Eq. (9) in its left hand side, we get

$$1-\frac{1}{J\gamma_0\langle S^z\rangle N}$$
$$\times\sum_{\mathbf{k}}\frac{Jb_1\gamma_0(1-\Gamma_{\mathbf{k}})\sinh(\beta h)-2\langle S^z\rangle\omega_{\mathbf{k}}^{\perp}\sinh(\beta\omega_{\mathbf{k}}^{\perp})}{\cosh(\beta h)-\cosh(\beta\omega_{\mathbf{k}}^{\perp})}\equiv R. \quad (27)$$

The quantity R is a function of field and temperature. Due to Eq. (22), expression (27) is singularity-free. It is evident that the closer R is to zero, the better the approximation. Thus, the condition $|R|\ll 1$ can serve as another criterion of the approximation efficiency. Below, in discussing the results, we will calculate $R(h,T)$ and check the fulfillment of this criterion for the proposed scheme.

Note that employing a similar approach for HFMs on a chain and a square lattice [below, we refer to it as the Green function approximate method (GFAM)], Junger *et al.*[39] instead of Eq. (22) used the condition $R=0$ as one of the equations in the self-consistent set of equations. In the following, we will compare the thermodynamic functions calculated within our scheme with the results found in Ref. 39.

III. RESULTS AND DISCUSSION

In the general case, the set of equations (23) can be solved only numerically. In limiting cases, analytical results could be obtained. At $T=0$, the system (23) gives correct values for the sought quantities

$$\langle S^z\rangle=\frac{1}{2}, \quad c_{1,2}=0, \quad a_1=1, \quad a_2=\gamma_0-1. \quad (28)$$

The same solution is also true for finite temperatures at $h\to\infty$.

In the high-temperature limit ($J,h\ll T$), the system (23) can be solved by expanding in $1/T$. Restricting our consideration to second order in $x=J/4T$ and $y=h/2T$, we obtain the following asymptotic expressions:

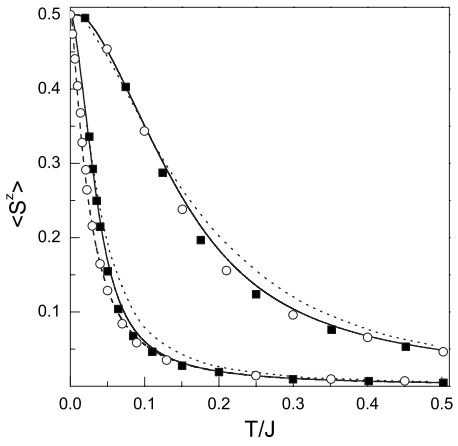

FIG. 1. Temperature dependences of the magnetization for 1D HFM at $h/J=0.005$ and 0.05 (from left to right). The infinite system: present theory (solid line), BA (Ref. 39) (■), and GFAM (Ref. 39) (dotted line). The cluster: present theory (dashed line) and ED (Ref. 39) (○).

$$c_1^{as}=x+\frac{x^2}{4}(\gamma_0^2-6\gamma_0+4),$$

$$c_2^{as}=\frac{x}{4}[(\gamma_0-2)(\gamma_0-4)-x(\gamma_0^2-14\gamma_0+20)],$$

$$a_1^{as}=c_1^{as}+y^2, \quad a_2^{as}=c_2^{as}+(\gamma_0-1)y^2,$$

$$\langle S^z\rangle^{as}=\frac{y}{2}(1+\gamma_0 x), \quad \alpha_z^{as}=\alpha_{\perp}^{as}=1-\frac{x}{3}. \quad (29)$$

For the heat capacity $C=dE/dT$ to third order in x and y, we get

$$C^{as}=\frac{3\gamma_0 x^2}{2}\left[1+\frac{x}{2}(\gamma_0^2-6\gamma_0+4)\right]+y^2(1+3\gamma_0 x). \quad (30)$$

The expressions for the magnetization and heat capacity coincide with those obtained by the direct high-temperature series expansion.[43] As it follows from Eq. (29), the field-dependent terms in expansions for c_l occur in the fourth or higher order in $1/T$.

We will demonstrate the efficiency of the proposed scheme, applying it to the 1D HFM and a HFM on a square lattice. The main attention is focused on low fields, because it is this region that is the most difficult to describe adequately within approximate methods.

A. One-dimensional Heisenberg model

In this section, we consider a 1D HFM. Figures 1–3 demonstrate the magnetization, susceptibility $\chi=\partial\langle S^z\rangle/\partial h$, and heat capacity vs temperature at low fields obtained within our approach. In calculating the thermodynamic functions on clusters, we use the periodic boundary conditions. The corresponding dependences found in Ref. 39 by Bethe ansatz (BA) and GFAM for an infinite chain and by the exact di-

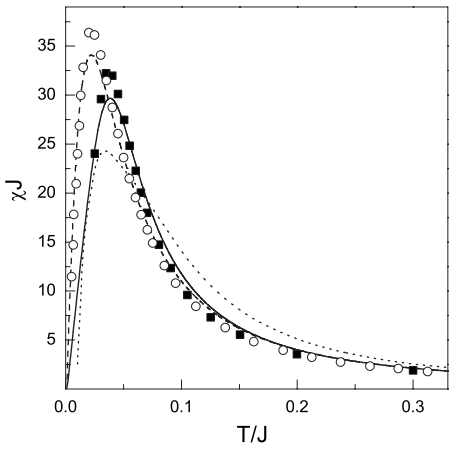

FIG. 2. Temperature dependences of the susceptibility for 1D HFM at $h/J=0.005$. The infinite system: present theory (solid line), BA (Ref. 39) (■), and GFAM (Ref. 39) (dotted line). The cluster: present theory (dashed line) and ED (Ref. 39) (○).

agonalization (ED) for a cluster of 16 sites are also shown for comparison.

For the magnetization and susceptibility, our method yields good agreement with the exact results in the whole temperature range. The positions of the maxima in our curves for $\chi(T)$ coincide perfectly with those found within the exact methods, and only a small difference in the peak heights is observed.

At low fields, the exact methods indicate the dependence of the thermodynamic functions on the chain length. As it is seen from Figs. 1 and 2, at $h/J=0.005$, the curves $\langle S^z(T)\rangle$ and $\chi(T)$ obtained by ED for the finite-sized chain differ substantially from those found by BA for the infinite system. Our method gives a proper description of this effect. At higher fields (Figs. 1 and 3) where the ED and BA results coincide, our dependences for $N=16$ and $N\to\infty$ also coincide and show a good fit to the exact data.

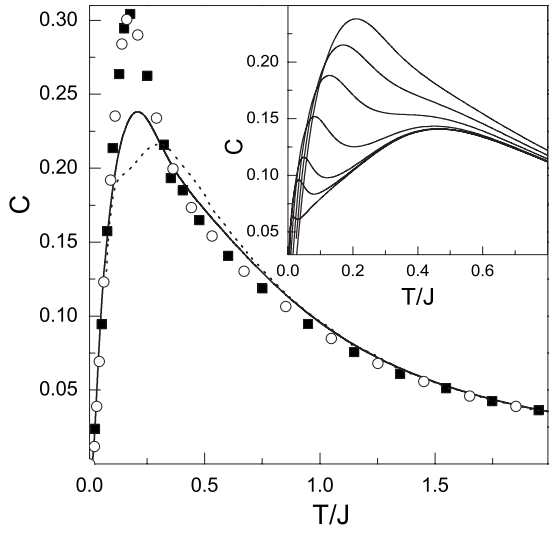

FIG. 3. Temperature dependences of the heat capacity for 1D HFM at $h/J=0.1$. The infinite system: present theory (solid line), BA (Ref. 39) (■), and GFAM (Ref. 39) (dotted line). The cluster: ED (Ref. 39) (○). The inset shows $C(T)$ at low fields $h/J=0.001$, 0.005, 0.01, 0.025, 0.05, 0.075, and 0.1 (from bottom to top).

As can be seen from Fig. 3, there is a certain disagreement between the heat capacities obtained within the exact and approximate methods at low fields. This result is quite understandable. Indeed, a similar scheme[33] applied to 1D HFMs at $h=0$ gives in the low-temperature region a sufficiently different run of the heat capacity than the exact solution. Nevertheless, even at $h/J=0.1$, our theory not only gives the correct position of the maximum but also reproduces a specific bend in the curve $C(T)$ at $T/J\sim 0.3$. The agreement between $C(T)$ calculated within our scheme and found by the exact methods becomes better with increase in field. The inset in Fig. 3 illustrates a double-peak structure of the heat capacity that within our method is identified at $0<h/J<0.045$. A similar structure of $C(T)$ at low fields was first obtained in Ref. 39.

We calculated the entropy for the 1D HFM. It turned out that the higher is the field, the closer is the limiting value $S(\infty)$ to $\ln 2$. For example, at $h/J=0.05$, the entropy is $S(\infty)\simeq 0.631$, and at $h/J=1$, it is $S(\infty)\simeq 0.687$. The quantity $R(h,T)$ was also found. At low and high temperatures, it is practically equal to zero, so that the Green function (9) and correlators calculated within our method may be considered as satisfying Eq. (26). At a given field in the intermediate temperature range where the correlators vary rapidly, the quantity R is at maximum. At $h/J=0.05$, the maximum value of R is ~ 0.027, whereas at $h/J=1$, it does not exceed 0.006. With increase in h/J, the quantity R decreases and the difference between results obtained by the exact and approximate methods vanishes.

B. Heisenberg ferromagnet on a square lattice

Now, we proceed to the HFM on a square lattice. Figure 4 demonstrates the magnetization as a function of temperature at $h/J=0.1$ and 0.4 for 4×4 and 32×32 square lattice clusters together with QMC,[41] ED,[39] and GFAM[39] data. The inset shows the magnetizations for the 32×32 cluster at $h/J=0.05$, 0.1, 0.2, 0.32, and 0.4 found within the present method, QMC,[41] and HTSE.[43] The comparison between our results and HTSE is possible, because at these values of field, the magnetizations for the 32×32 cluster proved[41] to be identical to those for the infinite lattice. It is seen that the temperature dependences of $\langle S^z\rangle$ obtained within our approach are in good agreement with the exact results. The proposed scheme reproduces correctly the dependence of $\langle S^z\rangle$ on the size of the system as well. The difference between the present results and GFAM in Fig. 4 (see also Figs. 1–3) testifies that Eq. (22) is more preferable as compared to the condition $R=0$ for a quantitative description of the low-dimensional HFM at small fields. It is also evident that the thermodynamic functions of the square lattice HFM are more sensitive to the choice of the condition for $\langle S^z\rangle$ than the thermodynamic functions for the 1D HFM. Naturally, such a choice is expected to be even more critical for the lattices with larger coordination numbers (for example, a triangular lattice).

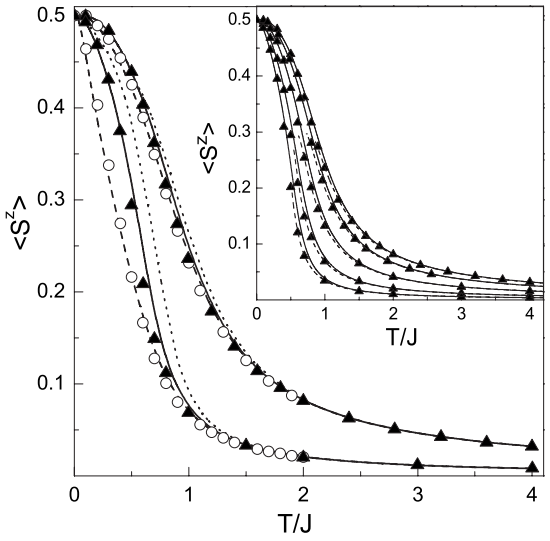

FIG. 4. Temperature dependences of the magnetization for HFM on a square lattice at $h/J=0.1$ and 0.4 (from left to right). The infinite system: present theory (solid line), QMC (Ref. 41) (▲), and GFAM (Ref. 39) (dotted line). The 4×4 cluster: present theory (dashed line) and ED (Ref. 39) (○). The inset shows $\langle S^z\rangle$ vs T/J at $h/J=0.05$, 0.1, 0.2, 0.32, and 0.4 (solid line) in comparison with QMC (Ref. 41) (▲) and HTSE (Ref. 43) (dashed line) (from left to right).

Figure 5 illustrates the susceptibility $\chi(T)$ for the square lattice together with $\chi(T)$ found by HTSE,[43] ED,[39] and GFAM.[39]

The temperature dependences of the correlation functions a_1 and c_1 at $h/J=0.1$ and 0.4 calculated for the 4×4 cluster as well as for the infinite lattice are presented in Fig. 6. The ED and GFAM results are added for comparison. At low fields, a clearly defined dependence on the size of the system is seen. Our results for the infinite lattice differ noticeably from GFAM. For the 4×4 cluster, good agreement with the dependences calculated by ED is observed.

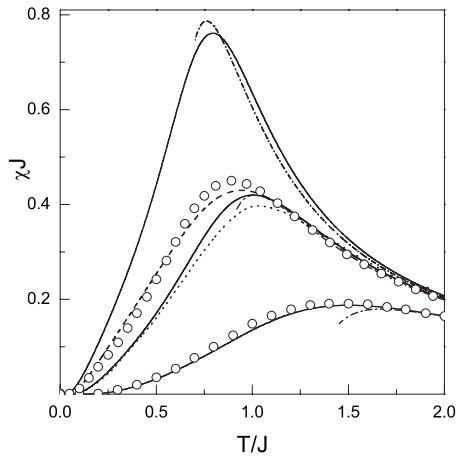

FIG. 5. Temperature dependences of the susceptibility for HFM on a square lattice at $h/J=0.2$, 0.4, and 1.0 (from top to bottom). The infinite system: present theory (solid line), HTSE (Ref. 43) (dash-dotted line), and GFAM (Ref. 39) (dotted line). The 4×4 cluster: present theory (dashed line) and ED (Ref. 39) (○).

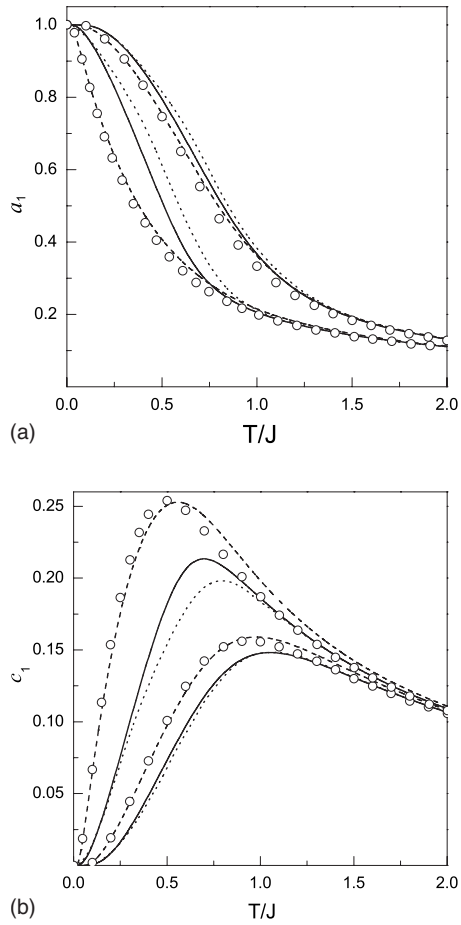

FIG. 6. Correlation functions (a) a_1 and (b) c_1 for HFM on a square lattice at $h/J=0.1$ and 0.4 (from left to right). The infinite system: present theory (solid line) and GFAM (Ref. 39) (dotted line). The 4×4 cluster: present theory (dashed line) and ED (Ref. 39) (○).

The limiting value of entropy for the HFM on the square lattice is $S(\infty)=0.651$ at $h/J=0.05$ and $S(\infty)=0.684$ at $h/J=1$, which is very close to the exact value of ln 2. The maximum value of R is $\simeq0.058$ at $h/J=0.05$ and $\simeq0.014$ at $h/J=1$.

Thus, the results of Secs. III A and III B show that the theory based on the correct accounting for the analytical properties of Green functions gives an adequate description of the thermodynamic functions for the systems under consideration in the wide field and temperature ranges.

C. Heisenberg ferromagnet on a triangular lattice

In this section, we consider a HFM on a triangular lattice in an external magnetic field with peculiar attention concentrated on small and intermediate fields. Figure 7 represents the temperature dependences of the magnetization at different values of h/J. It is seen that our results agree closely with HTSE[43] up to the point of HTSE applicability, whereas the RPA curves coincide with HTSE only at relatively high temperatures. In the intermediate temperature range, the RPA results differ significantly from ours even at $h/J=1.5$, repro-

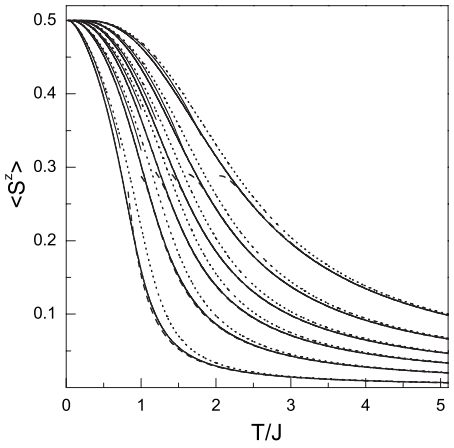

FIG. 7. Temperature dependences of the magnetization for HFM on a triangular lattice at $h/J=0.1$, 0.3, 0.5, 0.7, 1.0, and 1.5 (from left to right). The present theory (solid line), HTSE (Ref. 43) (dashed line), RGT (thin line), and RPA (dotted line).

ducing the temperature behavior of $\langle S^z \rangle$ only qualitatively. We have also calculated the magnetization at low temperatures using the renormalization group technique. The results obtained by both our approaches are in good agreement.

At a given magnetic field, the magnetization for the triangular lattice exceeds $\langle S^z \rangle$ for the square one within the whole temperature range. This result seems quite natural because the local field for a spin of the triangular lattice ferromagnet is higher than that for a spin of the square ferromagnet due to the greater coordination number of the triangular lattice.

Figure 8 illustrates the temperature behavior of the susceptibility. Analysis shows that with increase in field, the maximum in $\chi(T)$ decreases and shifts to higher temperatures. At $h/J \geqslant 0.1$, the height of the maximum as a function of h/J, with a great degree of accuracy, is described by a power law

$$\chi_{max} = a\left(\frac{h}{J}\right)^b, \quad a = 0.1696, \quad b = -0.8634. \qquad (31)$$

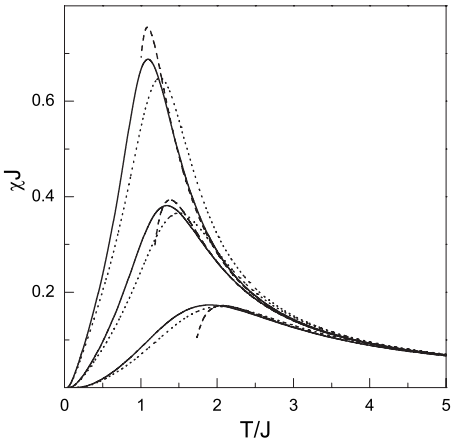

FIG. 8. Temperature dependences of the susceptibility for HFM on a triangular lattice at $h/J=0.2$, 0.4, and 1.0 (from top to bottom). The present theory (solid line), HTSE (Ref. 43) (dashed line), and RPA (dotted line).

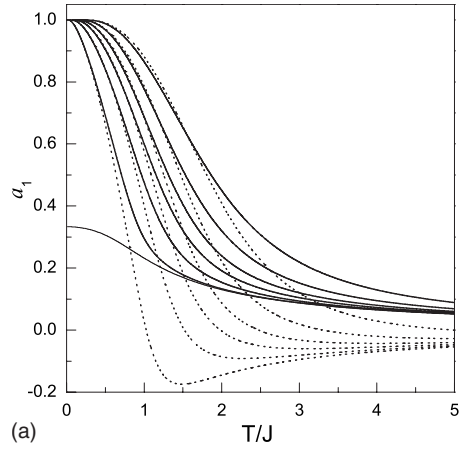

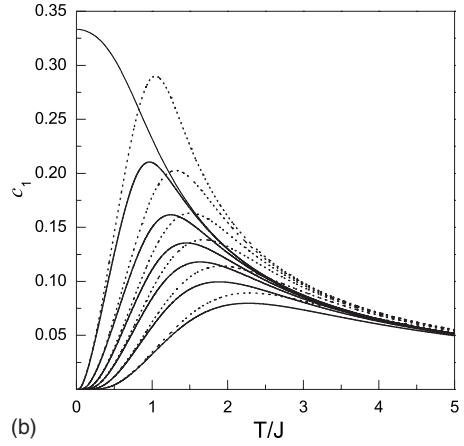

FIG. 9. Correlation functions (a) a_1 and (b) c_1 for HFM on a triangular lattice at $h/J=0.1$, 0.3, 0.5, 0.7, 1.0, and 1.5 (from left to right). The present theory (solid line) and RPA (dotted line). Thin lines correspond to $h=0$.

Temperature dependences of the correlation functions a_1 and c_1 at different h/J are shown in Fig. 9. Beginning with $T/J \sim 0.5$, the RPA results differ from ours sufficiently. It is easy to verify that at $T \gg J$, the correlator a_1 calculated within RPA to the first approximation in J/T is negative and equal to $-J/4T$. Thus, at almost all temperatures, RPA fails to describe correctly the correlation functions and, hence, the energy and heat capacity.

Figure 10 demonstrates the temperature dependences of the heat capacity $C(T)$ in comparison with HTSE[43] and RPA. It is seen that our results are in good agreement with HTSE. With increase in field, the position of the maximum in the curve $C(T)$ shifts to higher temperatures, and its value C_m^{tr} first increases rapidly and then decreases. A similar behavior occurs for the heat capacity maximum C_m^{sq} on a square lattice. Maximum values C_m^{sq} and C_m^{tr} vs field are illustrated in Fig. 11. Field dependences of the maximum positions for the square and triangular lattices are shown in the inset. At $h/J \leqslant 1$, both $C_m^{tr}(h/J)$ and $C_m^{sq}(h/J)$ can be approximated by a function

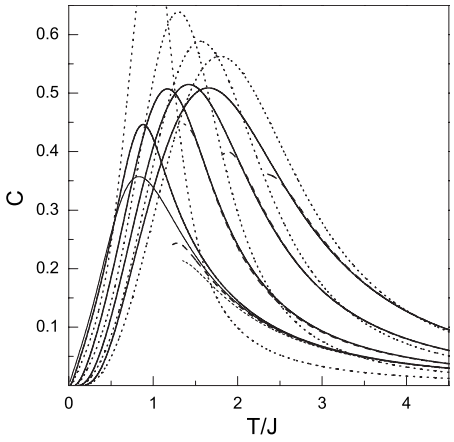

FIG. 10. Temperature dependences of the heat capacity for HFM on a triangular lattice at $h/J=0.1$, 0.5, 1.0, and 1.5 (from left to right). The present theory (solid line), HTSE (Ref. 43) (dashed line), and RPA (dotted line). Thin lines correspond to $h=0$.

$$C_m = \frac{ax}{b+x}, \quad x = \frac{h}{J},$$

with

$$a = \begin{cases} 0.5136 \\ 0.5254, \end{cases} \quad b = \begin{cases} 0.0239 & \text{square} \\ 0.0189 & \text{triangular.} \end{cases}$$

At higher fields ($h/J \geqslant 1.4$), the maximum values decrease linearly

$$C_m = Ax + B,$$

with

$$A = \begin{cases} -0.006\,93 \\ -0.0248, \end{cases} \quad B = \begin{cases} 0.5118 & \text{square} \\ 0.5468 & \text{triangular.} \end{cases}$$

Since C_m^{sq} decreases slower than C_m^{tr}, the inequality $C_m^{tr} > C_m^{sq}$ valid for low fields changes into the opposite one at $h/J \geqslant 2$.

Let us consider now the dependence of the thermodynamic functions on the cluster size $L \times L$. It is interesting to determine the linear size L_0 corresponding to the thermodynamic limit at a given magnetic field. This quantity is important, for example, when using such methods as Monte Carlo and exact diagonalization, when knowledge of an optimal cluster size makes it possible to obtain the thermodynamic functions of the infinite system within a reasonable volume of calculations. The dependence of the thermodynamic functions on L is also of practical interest, because of the isle structure of ^{3}He layers at some coverages.[24]

Figure 12 displays temperature dependences of the heat capacity at $h/J=0.1$ and 1 for different cluster sizes L up to L_0. It is seen that with decrease in L, the maximum in the curve $C(T)$ decreases and shifts to higher temperatures. At small L and very low fields, a second maximum resulting from the finite size of the system arises in the low-temperature part of the heat capacity. At higher fields, the Zeeman energy increases and suppresses the size effect

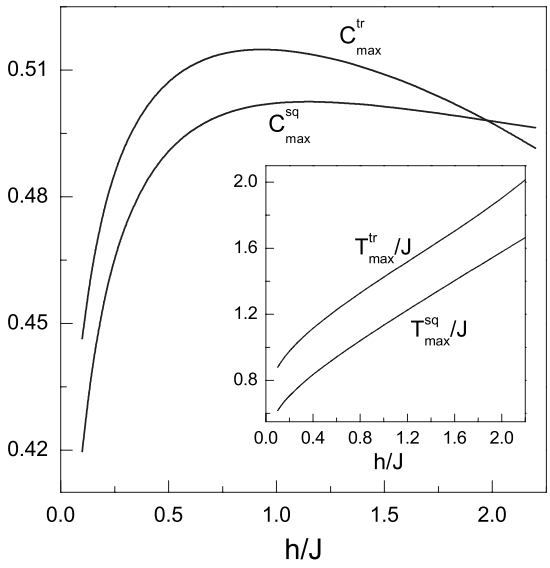

FIG. 11. Field dependences of the heights and positions of the heat capacity maxima for HFMs on square and triangular lattices.

caused by the boundary spins. A similar additional heat capacity maximum at small h was found by ED for the 4×4 square lattice in Ref. 39. This result is also reproduced by our calculations.

Figure 13 shows dependences $L_0(h/J)$ for the square and triangular lattices. At $h/J < 0.2$, even a small variation in field leads to a sufficient change in L_0. As the field increases, this dependence weakens, so that beginning with $h/J \sim 0.2$ rather small-sized clusters are appropriate for the numerical simulations of the real infinite systems.

Temperature dependences of the magnetization for a 16×16 triangular lattice together with the corresponding QMC data[44] are shown in Fig. 14. Our results agree well with QMC.

Now we check the two criteria outlined in Sec. II, as applied to the triangular lattice HFM. The limiting value of the entropy is equal to 0.708 and 0.713 at $h/J=0.05$ and 1,

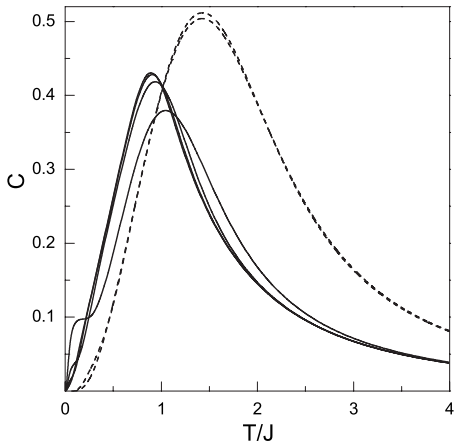

FIG. 12. Temperature dependences of the heat capacity for HFM on a triangular lattice (from bottom to top): $h/J=0.1$ and $L=4$, 6, 8, and 10 (solid line), and $h/J=1$ and $L=4$ and 6 (dashed line).

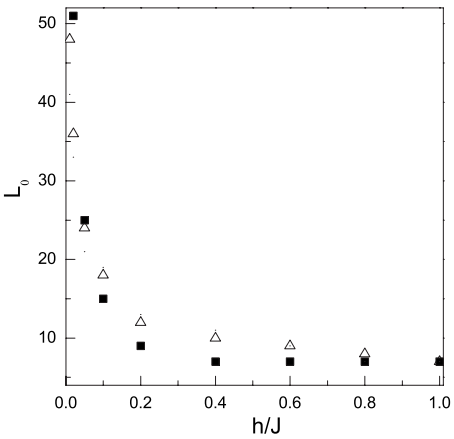

FIG. 13. Dependences $L_0(h/J)$ for triangular (△) and square (■) lattices.

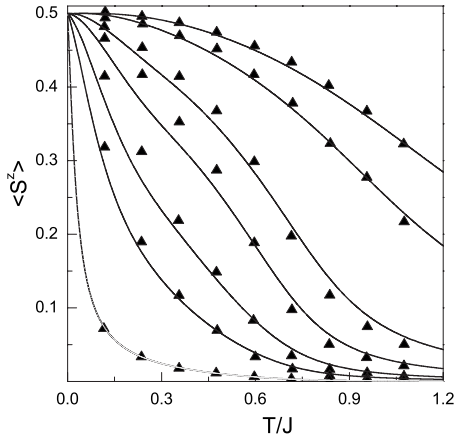

FIG. 14. Temperature dependences of the magnetization for 16×16 triangular lattice HFM at $h/J=0.429$, 0.214, 0.0429, 0.0171, 6.09×10^{-3}, 2.76×10^{-3}, and 4.29×10^{-4} (from top to bottom): present theory (solid line) and QMC (Ref. 44) (symbols).

respectively, which slightly exceeds ln 2. At low and high temperatures, the function $R(T,h)$ is close to zero as it was for HFMs on the chain and square lattice. At fixed field in the intermediate temperature region, $R(T,h)$ has a maximum, whose height decreases as h/J increases. The maximum value of R is ~0.094 at $h/J=0.05$, whereas at $h/J=1$, it does not exceed 0.046.

IV. SUMMARY

The thermodynamics of the low-dimensional spin-$\frac{1}{2}$ Heisenberg ferromagnets in an external magnetic field is investigated within a second-order two-time Green function formalism in the wide temperature and field ranges. The self-consistent set of equations for the correlation functions, vertex parameters, and magnetization is obtained in the universal form appropriate for the description of low-dimensional HFMs on a chain and square and triangular lattices. The fundamental point of our consideration is the account of the correct analytical properties for the approximate transverse commutator Green function, from which the equation for the magnetization follows. This enables us to extend the range of adequate description for the HFM thermodynamics to lower fields as compared to the scheme proposed in Ref. 39.

The thermodynamics of a triangular lattice HFM in a magnetic field is studied within a second-order Green function formalism. The temperature dependences of the magnetization, susceptibility, correlation functions, and heat capacity at different values of the magnetic field are calculated and analyzed in detail. For square and triangular lattices, the positions and heights of the heat capacity maxima vs field are obtained. The dependences of the thermodynamic functions of the 2D HFM on the cluster size are investigated. For both types of lattices, the cluster sizes corresponding to the thermodynamic limit are found as functions of field.

The temperature and field dependences for the thermodynamic functions calculated within our scheme are in close agreement with the corresponding results obtained by Bethe ansatz, quantum Monte Carlo simulations, high-temperature series expansion, and exact diagonalization. Thus, we can conclude that the scheme used in this paper provides a good quantitative description for the thermodynamics of the low-dimensional HFM in an external magnetic field on the three considered types of lattices for infinite as well as for finite-sized systems.

*chishko@ilt.kharkov.ua

[1] M. Tamura, Y. Nakazawa, K. Nozawa, Y. Hosokoshi, M. Ishikawa, M. Takahashi, and M. Kinoshita, Chem. Phys. Lett. **186**, 401 (1991).
[2] P. Turek, K. Nozawa, D. Shiomi, K. Awaga, T. Inabe, Y. Maruyama, and M. Kinoshita, Chem. Phys. Lett. **180**, 327 (1991).
[3] Y. Nakazawa, M. Tamura, N. Shirakawa, D. Shiomi, M. Takahashi, M. Kinoshita, and M. Ishikawa, ISSP Technical Report No. 2521, 1992 (unpublished).
[4] M. Takahashi, P. Turek, Y. Nakazawa, M. Tamura, K. Nozawa, D. Shiomi, M. Ishikawa, and M. Kinoshita, Phys. Rev. Lett. **67**, 746 (1991).
[5] M. Takahashi, M. Kinoshita, and M. Ishikawa, ISSP Technical Report No. 2544, 1992 (unpublished).
[6] C. P. Landee and R. D. Willett, Phys. Rev. Lett. **43**, 463 (1979).
[7] R. D. Willett, C. P. Landee, R. M. Gaura, D. D. Swank, H. A. Groenendijk, and A. J. Van Duyneveldt, J. Magn. Magn. Mater. **15–18**, 1055 (1980).
[8] S. Feldkemper and W. Weber, Phys. Rev. B **57**, 7755 (1998).
[9] S. Feldkemper, W. Weber, J. Schulenburg, and J. Richter, Phys. Rev. B **52**, 313 (1995).
[10] H. Manaka, T. Koide, T. Shidara, and I. Yamada, Phys. Rev. B **68**, 184412 (2003).
[11] S. E. Barrett, G. Dabbagh, L. N. Pfeiffer, K. W. West, and R. Tycko, Phys. Rev. Lett. **74**, 5112 (1995).

[12] N. Read and S. Sachdev, Phys. Rev. Lett. **75**, 3509 (1995).
[13] M. J. Manfra, E. H. Aifer, B. B. Goldberg, D. A. Broido, L. Pfeiffer, and K. West, Phys. Rev. B **54**, R17327 (1996).
[14] D. S. Greywall, Phys. Rev. B **41**, 1842 (1990).
[15] O. E. Vilches, R. S. Ramos, Jr., and D. A. Ritter, Czech. J. Phys. **46**, 397 (1991).
[16] M. Siqueira, J. Nyéki, B. Cowan, and J. Saunders, Phys. Rev. Lett. **76**, 1884 (1996).
[17] M. Siqueira, J. Nyéki, B. Cowan, and J. Saunders, Phys. Rev. Lett. **78**, 2600 (1997).
[18] M. Morishita, K. Ishida, K. Yawata, and H. Fukuyama, Czech. J. Phys. **46**, 409 (1996).
[19] K. Ishida, M. Morishita, K. Yawata, and H. Fukuyama, Phys. Rev. Lett. **79**, 3451 (1997).
[20] C. Bäuerle, J. Bossy, Yu. M. Bunkov, A.-S. Chen, and H. Godfrin, J. Low Temp. Phys. **110**, 345 (1998).
[21] M. Roger, C. Bäerle, Yu. M. Bunkov, A.-S. Chen, and H. Godfrin, Phys. Rev. Lett. **80**, 1308 (1998).
[22] C. Bäuerle, Yu. M. Bunkov, S. N. Fisher, and H. Godfrin, Czech. J. Phys. **46**, 399 (1996).
[23] C. Bäuerle, J. Bossy, Yu. M. Bunkov, A.-S. Chen, H. Godfrin, and M. Roger, J. Low Temp. Phys. **110**, 345 (1998).
[24] H. Godfrin and R. E. Rapp, Adv. Phys. **44**, 113 (1995).
[25] T. N. Antsygina and K. A. Chishko, J. Low Temp. Phys. **119**, 677 (2000).
[26] A. Yamaguchi, T. Watanuki, R. Masutomi, and H. Ishimoto, J. Low Temp. Phys. **138**, 307 (2005).
[27] M. Neumann, J. Nyéki, B. P. Cowan, and J. Saunders, J. Low Temp. Phys. **138**, 391 (2005).
[28] D. N. Zubarev, *Nonequilibrium Statistical Thermodynamics* (Consultant Bureau, New York, 1974).
[29] Yu. G. Rudoi, *Statistical Physics and Quantum Field Theory* (Nauka, Moscow, 1973), in Russian.
[30] W. Gasser, E. Heiner, and K. Elk, *Greensche Funktionen in Festkörper—und Vielteilchenphysik* (Wiley-VCH Verlag, Berlin, 2001).
[31] P. Fröbrich and P. J. Kuntz, Phys. Rep. **432**, 223 (2006).
[32] S. V. Tjablikov, *Methods in the Quantum Theory of Magnetism* (Plenum, New York, 1967).
[33] J. Kondo and K. Yamaji, Prog. Theor. Phys. **47**, 807 (1972).
[34] K. Yamaji and J. Kondo, Phys. Lett. **45A**, 317 (1973).
[35] H. Shimahara and S. Takada, J. Phys. Soc. Jpn. **60**, 2394 (1991).
[36] T. N. Antsygina and V. A. Slusarev, Low Temp. Phys. **19**, 48 (1993).
[37] T. N. Antsygina and V. A. Slusarev, Low Temp. Phys. **21**, 93 (1995).
[38] T. N. Antsygina, Low Temp. Phys. **25**, 440 (1999).
[39] I. Junger, D. Ihle, J. Richter, and A. Klümper, Phys. Rev. B **70**, 104419 (2004).
[40] M. Takahashi, Phys. Rev. B **44**, 12382 (1991).
[41] P. Henelius, A. W. Sandvik, C. Timm, and S. M. Girvin, Phys. Rev. B **61**, 364 (2000).
[42] H. Nakamura and M. Takahashi, J. Phys. Soc. Jpn. **63**, 2563 (1994).
[43] G. A. Baker, Jr., H. E. Gilbert, J. Eve, and G. S. Rushbrooke, Phys. Lett. **25A**, 207 (1967).
[44] P. Kopietz, P. Scharh, M. S. Skaf, and Chakravarty, Europhys. Lett. **9**, 465 (1989).
[45] H. Godfrin, R. R. Ruel, and D. D. Osheroff, J. Phys. (Paris), Colloq. **C8**, 2045 (1988).
[46] E. V. L. de Mello and H. Godfrin, J. Low Temp. Phys. **108**, 407 (1997).